Nanoscale

PAPER

View Article Online
View Journal

Cite this: DOI: 10.1039/d1nr00619c

Gold cluster-loaded dendritic nanosilica: single particle luminescence and catalytic properties in the bulk†

Jyoti Sarita Mohanty,[a] Ayan Maity,[b] Tripti Ahuja,[a] Kamalesh Chaudhari,[a] Pillalamarri Srikrishnarka,[a] Vivek Polshettiwar[b] and Thalappil Pradeep *[a]

Received 29th January 2021,
Accepted 6th May 2021

DOI: 10.1039/d1nr00619c

rsc.li/nanoscale

We report a hybrid material in which surface anchoring-induced enhanced luminescence of Au_{QC}@BSA clusters on high surface area dendritic fibrous nanosilica of 800 nm diameter enabled their luminescence imaging at a single particle level. The photophysical and structural properties of the hybrid material were characterized by various spectroscopic and microscopic techniques. Concomitant imaging using scattering and luminescence of such mesostructures and their response to analytes have been used to develop a chemical sensor. The hybrid material was found to be catalytically active in silane to silanol conversion, and 100% conversion was observed in 4 h when the reaction was carried out at 30 °C in the presence of light. Such materials at submicron dimensions with enhanced surface area, emission in the solid state along with a high quantum yield of 12% in water along with enhanced scattering, and surface functionalities present numerous benefits for the creation of multifunctional materials.

Introduction

Atomically precise noble metal nanoclusters owing to their fascinating physical and chemical properties have been studied extensively.[1–5] Different ligands such as thiols,[6] DNA,[7,8] dendrimers,[9] and proteins[3] have been used for synthesizing such sub-nanometer-sized clusters. Among them, use of proteins as ligands is emerging as a result of the simple synthetic procedure employed in cluster synthesis and due to their biocompatible nature and promising applications. Bovine serum albumin (BSA),[10,11] Lactoferrin (Lf),[12] Lysozyme (Lyz),[13,14] *etc.*, are the commonly used proteins for synthesizing noble metal nanoclusters. Intense photoluminescence, high quantum yield, and stability over a wide range of pH make them suitable candidates in the field of sensors.[15]

Protein protected clusters (PPCs) are sensitive to specific metal ions. Xie *et al.* reported the sensing of Hg^{2+} using BSA-protected gold clusters (Au_{QC}@BSA) for the first time.[16] The subscript, QC is used to indicate a quantum cluster, to ensure that these are distinctly different from BSA protected plasmonic nanoparticles. Subsequently, several other groups have demonstrated sensing of heavy metal ions like Cu^{2+}, Hg^{2+}, and Pb^{2+} using PPCs.[3,5,17,18] Mercury is one of the most hazardous environmental contaminants among other heavy metal ions. It is toxic both in the inorganic and organic forms.[19] Different methods have been developed to determine trace levels of Hg^{2+}. Luminescent PPCs are suitable candidates for approaching such problems.

Anchoring such cluster systems on suitable substrates can extend their applications in the field. A few attempts have also been made in this direction using a variety of hybrid materials. Binding of Au_{QC}@BSA to nanofibers was demonstrated by Ghosh *et al.* and they have used it for the detection of Hg^{2+}.[20] A CdTe@SiO_2 hybrid sphere was synthesized by Wang *et al.*, where Au_{QC}@BSA was covalently linked to the hybrid sphere through EDC chemistry and used it as a ratiometric fluorescent probe for the determination of Cu^{2+}.[21] Mohammed *et al.* have shown simultaneous sensing and scavenging of heavy metal ions using an Au_{QC}@BSA-cellulose nanocrystal (CNC) composite.[22] Adsorption of heavy metal ions by the composite showed a visible change in the color. Recently, Upadhyay *et al.* synthesized porous, pH responsive Au_{QC}@BSA hydrogel beads which were used for the removal of heavy metal cations from contaminated water.[23]

Silane to silanol chemistry has been used in organic synthesis for industrial applications to prepare silicon based pre-

[a]DST Unit of Nanoscience (DST UNS), and Thematic Unit of Excellence (TUE), Department of Chemistry, Indian Institute of Technology Madras, Chennai-600 036, India. E-mail: pradeep@iitm.ac.in
[b]Department of Chemical Sciences, Tata Institute of Fundamental Research (TIFR), Mumbai-400 005, India

†Electronic supplementary information (ESI) available: Zeta potential and UV-Vis absorption spectra of DFNS@Au_{QC}BSA, HRTEM images showing the structural evolution during the formation of DFNS@Au_{QC}BSA, XRD pattern, time dependent PL spectra of DFNS@Au_{QC}BSA, AFM phase imaging of DFNS and DFNS@Au_{QC}BSA, optical and fluorescence images of DFNS, the effect of light in the catalytic reaction at 45 °C and UV-Vis absorption spectra of DFNS@Au_{QC}BSA after catalytic reaction. See DOI: 10.1039/d1nr00619c

cursors.[24] The traditional way for synthesizing these silanol molecules is *via* hydrolysis of halosilanes, by reacting siloxanes with alkali substrates or by controlled oxidation of organosilanes.[25] Among them, the stoichiometric oxidation of silane with water is environmentally friendly. The reaction not only produces silanols with improved selectivity but also releases hydrogen which is also a useful by-product, although conducting this reaction at lower temperature is always a synthetic challenge.[26] Dendritic fibrous nanosilica (DFNS)[27] is a mesosphere with thin sheet-like fibers of 3.5 to 5.2 nm thickness. It possesses radially oriented fibrous channels with variable pore sizes ranging from 3 nm to 25 nm. Such dendritic fibrous morphology with a high surface area and better chemical and thermal stability made them distinctive from the conventional mesoporous silica materials. Until now, there have been no reports on DFNS-based luminescent materials using protein protected clusters. Herein, for the first time, we have synthesized a hybrid material, DFNS@ Au_{QC}BSA by anchoring luminescent Au_{QC}@BSA on the DFNS substrate. It has been shown before that adhesion on substrates increases luminescence of protein protected clusters.[20,22] The hybrid material was capable of sensing Hg^{2+} and was found to be catalytically active for silane to silanol conversion.

Experimental

Materials

Bovine serum albumin (BSA) at pH 6–7 was purchased from SRL Chemical Co. Ltd, India. Tetrachloroauric acid trihydrate ($HAuCl_4 \cdot 3H_2O$) was purchased from CDH, India. Tetraethyl orthosilicate, 3-aminopropyl triethoxysilane and sinapic acid were purchased from Sigma Aldrich, India. Urea, *p*-xylene, and sodium hydroxide (NaOH) were purchased from Rankem, India. Sodium borohydride ($NaBH_4$) was purchased from Spectrochem, India. Cetyl trimethyl ammonium bromide (CTAB) was purchased from Fluka, India. All the chemicals were used without further purification.

Instrumentation

UV-Vis spectra were collected using a PerkinElmer Lambda 25 instrument in the range of 200–1100 nm. Luminescence measurements were carried out on a Jobin Yvon NanoLog instrument. The band pass for excitation and emission was set as 3 nm. X-ray photoelectron spectroscopy (XPS) studies were conducted with an Omicron ESCA probe spectrometer with polychromatic Mg Kα X-rays ($h\nu$ = 1253.6 eV). The samples were spotted as drop-cast films on a sample stub. A constant analyser energy of 20 eV was used for the measurements. High resolution transmission electron microscopy (HRTEM) was performed with a JEOL 3010 instrument working at 300 kV, equipped with an ultra high resolution (UHR) pole piece. Energy dispersive X-ray analysis (EDS) was carried out with an Oxford EDAX housed in the TEM. A sample for HRTEM was prepared by dropping the dispersion on a carbon coated copper grid and drying under ambient conditions. High resolution scanning electron microscopy (HRSEM) images were collected using a Quanta 200 FEG SEM. Depending upon the compatibility of the sample, the instrument can work on three different operating modes namely, the high vacuum mode, low vacuum mode and environmental scanning electron microscope mode. For imaging purpose, samples were spotted on an indium tin oxide (ITO) conducting glass substrate and dried under ambient conditions. Atomic force microscopy (AFM) images were obtained using the asylum research Cypher ES AFM. Tapping mode (AC mode) was used for the measurement. X-ray diffraction (XRD) data were collected with a Bruker AXS, D8 discover diffractometer using Cu-Kα (λ = 1.54 Å) radiation. The diffractogram was collected from 5–100 degree 2θ range. Dark-field imaging of the hybrid material was performed using an Olympus BX-51 microscope and a 100 W quartz halogen light source on a Cyto Viva microscope setup. A broadband white light was used for the imaging purpose *via* a dark field condenser and a 100× oil immersion objective was used for collecting the scattered/emitted light from the particle. Imaging was performed using a true-color charge-coupled device (CCD). Hyperspectral image analysis software was used for spectral analysis and a mercury lamp was used for fluorescence images. GC-MS study was carried out using an Agilent 7890B instrument. For the light induced catalysis reaction, a Xe lamp of range 385–740 nm (Power 250 mW cm^{-2}) wavelength was used.

Synthesis

Synthesis of DFNS. Dendritic fibrous nanosilica (DFNS) was synthesized following a previously reported method.[28] The reaction was carried out using a 2 L four-neck round-bottom (RB) flask under refluxing conditions with a water condenser. In a typical synthesis, CTAB (10 g, 0.027 mol) and urea (12 g, 0.2 mol) were dissolved in 500 mL of water and mixed at 700 rpm using a magnetic stirrer for 30 minutes at room temperature. To the above solution, TEOS (50 mL, 0.24 mol) in 500 mL of *p*-xylene was added dropwise over 30 minutes under stirring. This reaction mixture was further stirred for 30 minutes. Then, 1-pentanol (30 mL) was added slowly into the reaction mixture and stirred for 30 minutes. The reaction mixture was heated to 130 °C (oil bath temperature) during 30 minutes ramp up and refluxed for 6 h under stirring at 700 rpm. After cooling, the solid product was isolated *via* centrifugation and washed several times with water and ethanol. After drying for 12 h at 80 °C, CTAB was removed by calcination at 550 °C for 6 h in air.

Synthesis of APTS functionalized DFNS. Functionalization of DFNS was performed following the reported method.[29] In brief, grafting of APTS was carried out by refluxing 2 g of calcined DFNS with 3-aminopropyl triethoxysilane (2 mL, 8.5 mM) in 250 mL of toluene at 80 °C for 24 h. The resulting material was washed repeatedly with toluene and ethanol followed by drying under vacuum at 60 °C for 12 h. The obtained material was APTS functionalized DFNS.

Synthesis of the hybrid material, DFNS@ Au_{QC}BSA. In a typical synthesis, 20 mg of BSA in 0.5 mL DI H_2O was added

into 8 mg of APTS functionalized DFNS in 0.5 mL DI H_2O under vigorous stirring. After 5 minutes, 6 mM $HAuCl_4$ was added to the above mixture followed by the addition of 150 μL 1 M NaOH. The reaction mixture was stirred vigorously until the solution turned golden brown in color. The change in color indicated the formation of clusters. The reaction was carried out for 10 h at room temperature. The sample was centrifuged, and the residue was washed with DI H_2O and this process was followed repeatedly to ensure the removal of unbound clusters from the solution. Then the final residue was used for various characterization studies.

Oxidation of silanes by DFNS@Au_{QC}BSA

About 5 mg DFNS@Au_{QC}BSA was placed in a 10 mL round bottom test-tube. To the reaction tube, a mixture of tetrahydrofuran (1 mL), water (30 μL) and silane [dimethylphenylsilane (230 μL, 1.5 mM), triisopropylsilane (307 μL, 1.5 mM), tributylsilane (385 μL, 1.5 mM) and triphenylsilane (391 mg, 1.5 mM)] was added and the reaction mixture was vigorously stirred at required temperature. The reaction was monitored by taking aliquots at different intervals of time and the products were determined by GC-MS analysis.

Results and discussion

Synthesis and characterization of the hybrid material, DFNS@Au_{QC}BSA

The hybrid material, DFNS@Au_{QC}BSA, made of Au_{QC}BSA and DFNS was synthesized by a two-step procedure. In the first step, BSA was covalently linked to the amine functionalized DFNS in an aqueous medium to form a DFNS-BSA complex and in the next step, $HAuCl_4$ was added to the above complex at alkaline pH (Fig. 1A). BSA acted as both reducing and stabilizing agents during the synthesis of Au_{QC}@BSA.[10] Basically, when $HAuCl_4$ is added to BSA, it forms a complex through its various functional groups and reduces Au^{3+} to Au^{+} and further reduction of Au^{+} to its metallic state is achieved at alkaline pH. The DFNS-BSA-$HAuCl_4$ complex at pH ~ 12 was allowed to stir at room temperature. After 4 h, the turbid reaction mixture started changing its color from yellowish to light brown and finally turned to golden brown after 10 h of reaction. Change in color indicated the formation of the cluster on DFNS. The nanosized pores and fibrous morphology of DFNS provided an efficient template for the encapsulation of sub-nanometer sized Au_{QC}@BSA. To observe the structural changes, FESEM and HRTEM studies were performed for both parent DFNS and the hybrid material. Fig. 1(B, C) and (F, G) represent the FESEM and HRTEM images of the parent DFNS, respectively. DFNS is dendritic mesospheres of diameter ~800 nm with increasing fibrous morphology towards the outer surface and is of uniform size. After 10 h of reaction, FESEM and HRTEM studies of the hybrid material were carried out and are shown in Fig. 1(D, E) and (H, I), respectively.

Incorporation of clusters on DFNS gave rise to a well-defined structure, where the clusters were uniformly dispersed towards the outer surface of the DFNS and appeared as a ring-like pattern. Distinct morphological changes were observed in DFNS@Au_{QC}BSA compared to the parent DFNS but no significant change in their size could be observed from both FESEM and HRTEM studies. It suggested that incorporation of the clusters on the DFNS did not bring any change in the overall

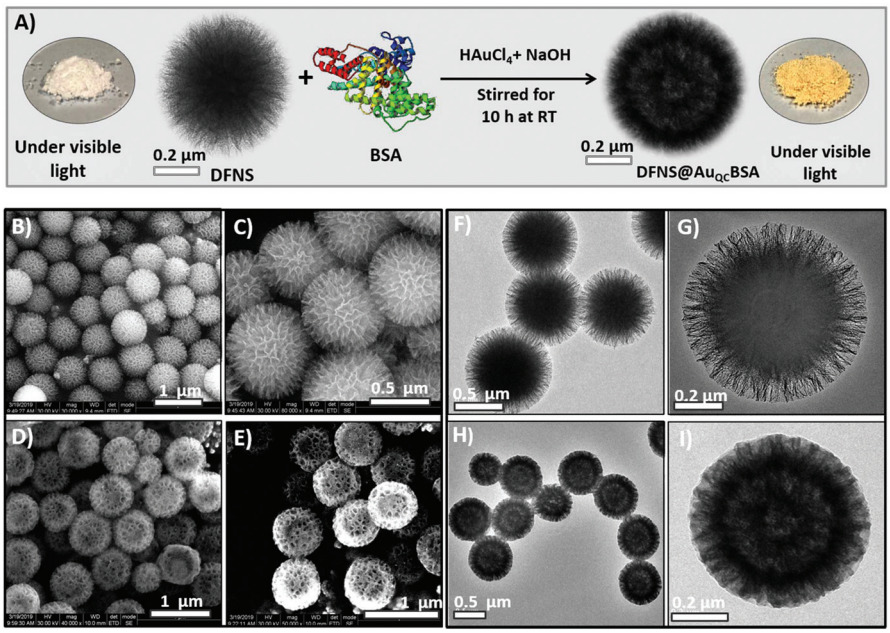

Fig. 1 (A) Schematic illustration showing the synthetic process leading to the hybrid material, DFNS@Au_{QC}BSA. (B and C) and (D and E) are the FESEM images of DFNS and DFNS@Au_{QC}BSA, respectively. (F and G) and (H and I) are the HRTEM images of DFNS and DFNS@Au_{QC}BSA, respectively. A well-defined morphological change was observed in DFNS@Au_{QC}BSA.

size or shape of the material. As the sizes of the clusters were less than 2 nm, they were difficult to be observed from the HRTEM images of the hybrid material. Isolated Au_{QC}BSA clusters were not prepared in solution, but they were investigated before.[3,10] The core size of such clusters was found to be less than 2 nm.[30,31]

UV-Vis and zeta potential study of DFNS@Au_{QC}BSA

Surface modification of DFNS helped to conjugate BSA onto it effectively and this was achieved through APTS functionalization, by replacing the hydroxyl groups (–OH) of DFNS with the amine ($–NH_2$) groups. This was monitored by measuring zeta potential of DFNS which was changed from −16.9 mV to +19.3 mV after functionalization. The binding of BSA to the amine functionalized DFNS was confirmed from the surface charge of −26.1 mV and it reached −34.7 mV after 10 h, which confirmed the binding and encapsulation of the cluster on DFNS (Fig. S1A†). To evaluate the changes in the optical properties during the formation of the hybrid material, UV-Vis spectra were collected (Fig. S1B†). BSA has a sharp absorption feature at 280 nm due to the presence of aromatic amino acid residues while DFNS did not show any absorption feature in the 300–800 nm range. A slight decrease in the absorption peak along with a gradual increase in absorbance from 800 nm was found in the DFNS-BSA complex, which suggested the conjugation of the protein onto DFNS. After 10 h of the reaction, the absorption feature at 280 nm decreased significantly along with a slope around 375 nm which confirmed the formation of clusters inside the protein template and proved successful incorporation of the cluster on DFNS.

Evolution of DFNS@Au_{QC}BSA

To understand the evolution of the hybrid material, time dependent HRTEM studies were conducted. Control experiments were also performed to know the effect of NaOH on DFNS during the synthesis (Fig. S2†). Addition of NaOH into the solution of DFNS induced a drastic morphological change due to etching of the surface (Fig. S2B†). But when NaOH was added into the DFNS-BSA complex, similar morphological changes were not observed; it was due to the conjugation of BSA on the fibrous channels of DFNS which prevented the etching of the DFNS surface (Fig. S2C†). During *in situ* synthesis of the cluster, $HAuCl_4$ was added to the DFNS-BSA complex followed by the addition of NaOH into the mixture. Although formation of the cluster started after 4 h of the reaction (started to show luminescence under UV light), visible morphological changes were not observed compared to the parent DFNS (Fig. S2D†). But after 6 h, the structure of the hybrid material started to emerge (Fig. S2E†) and a well-defined pattern with uniform arrangement of clusters towards the periphery of DFNS was observed post 10 h of the reaction (Fig. S2F†). During the reaction, a slight etching from the surface of the material was seen. We have already mentioned that the formation of clusters occurs only at alkaline pH. Therefore, here NaOH played a major role in reducing the gold ions in the cluster synthesis rather than only interacting with the surface of DFNS and this could be the reason for minimal surface etching seen in the hybrid material as compared to the parent DFNS. According to our earlier report, sizes of BSA and the cluster (including the protein shell) were found to be around 7.3 and 9 nm, respectively.[32] As the pore sizes of the DFNS decrease from the outer surface towards the center, BSA could easily enter into the compatible pore of the DFNS. A probable mechanism for the formation of DFNS@Au_{QC}BSA could be explained on the basis of dendritic fibrous morphology with varying pore sizes of DFNS which made it accessible for the conjugation of BSA (through its various functional groups) on DFNS from all the directions followed by the formation of the cluster with the addition of $HAuCl_4$ into alkaline medium. The reduced pore sizes towards the center of the DFNS restricted the entry of BSA as well as the growth of the cluster around the center which resulted in the formation of ring patterns near the edges of DFNS.

HRTEM EDS analysis of DFNS@Au_{QC}BSA

The incorporation of clusters on DFNS was confirmed further using HRTEM EDS elemental mapping (Fig. 2). The EDS map of Au L clearly showed a uniform dispersion of the cluster only at the edge while Si was nearly absent on that specific region as shown in the Si K map. The presence of silica was observed at the center of the hybrid material, where Au was nearly absent. Distribution of oxygen in O K was found similar to that of the Si K map and dispersion of S in the S K map matched well with the Au L map as the source of sulphur was from the protein. These data confirmed the presence of clusters as well as their uniform distribution at the edges of the hybrid material as speculated in the earlier section. Fig. 2F provides the quantification data of the hybrid material.

The powder X-ray diffraction (PXRD) pattern of DFNS showed a diffraction peak at $2\theta = 22.5°$ and BSA showed two diffraction peaks at $2\theta = 9°$ and $2\theta = 20.5°$ related to its crystalline nature (Cu Kα). The obtained values matched with the values reported.[29,33] For the hybrid material, very weak and broad peaks around $2\theta = 38°$ and 64° along with the one at $2\theta = 22.5°$ were observed, due to Au (111), Au (220) and amorphous SiO_2, respectively (Fig. S3†).

Photoluminescence properties of DFNS@Au_{QC}BSA

DFNS@Au_{QC}BSA showed strong red emission both in the solution and solid state indicating effective incorporation of clusters on DFNS, which were responsible for the strong luminescence exhibited by the hybrid material. DFNS@Au_{QC}BSA showed an emission maximum of ~640 nm with two excitation maxima around 365 and 500 nm (Fig. 3A). The photographs of the hybrid material in the aqueous solution under visible and UV light are shown in the inset of Fig. 3A. The material was freeze dried into a powder form and the powders also showed bright luminescence under UV light (Fig. 3B). A similar excitation maximum was observed for both solid and solution states. But a red shift from 640 to 645 nm was observed in the emission maximum of the solid material. This shift was attributed to the confinement of the cluster in the solid form.

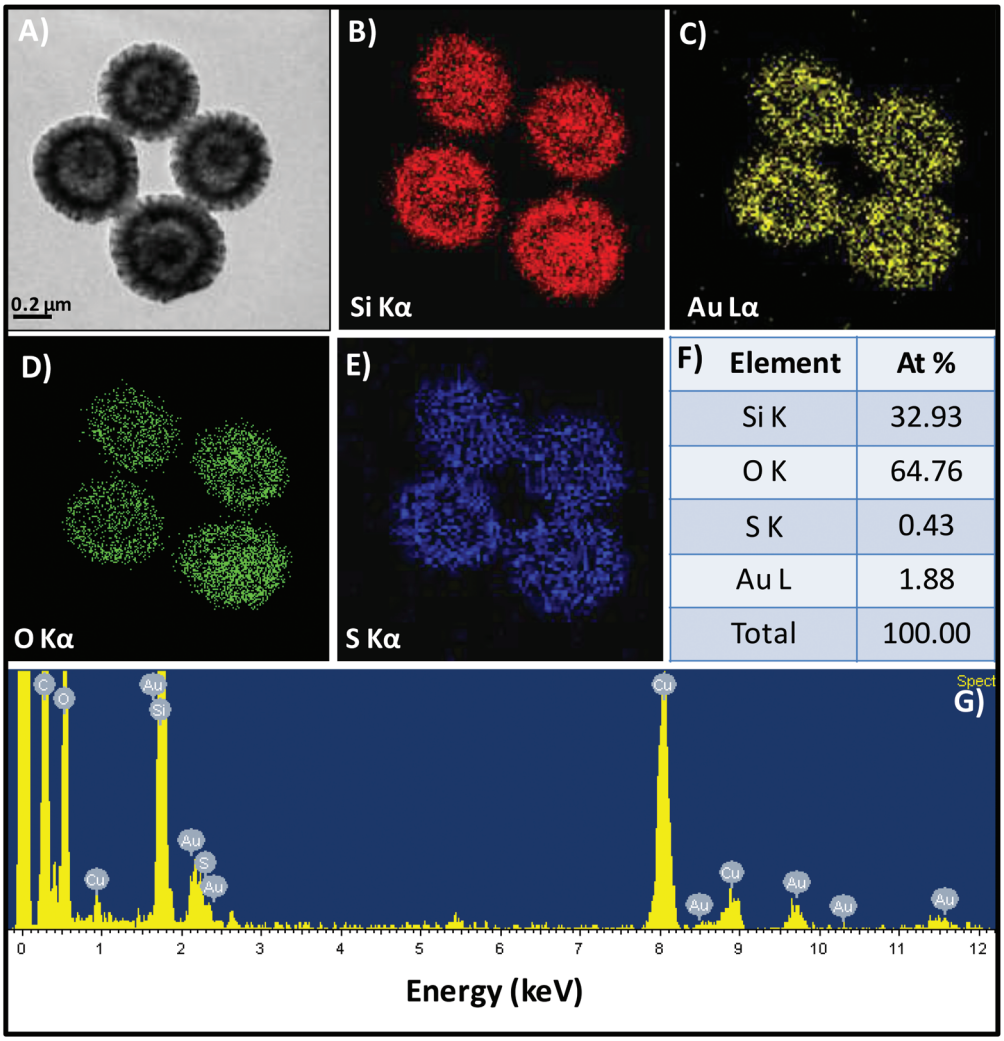

Fig. 2 EDS analysis to confirm the presence of clusters in the DFNS@Au_{QC}BSA. (A) TEM image of the hybrid material and the corresponding Si Kα, Au Lα, O Kα, and S Kα maps are shown in B, C, D and E, respectively. Au Lα mapping shows the presence of gold only at the edges of the sphere while the absence of silica from those regions is clearly seen from the Si Kα map. Quantification data and EDS spectrum showing the presence of expected elements in DFNS@Au_{QC}BSA are presented in F and G, respectively.

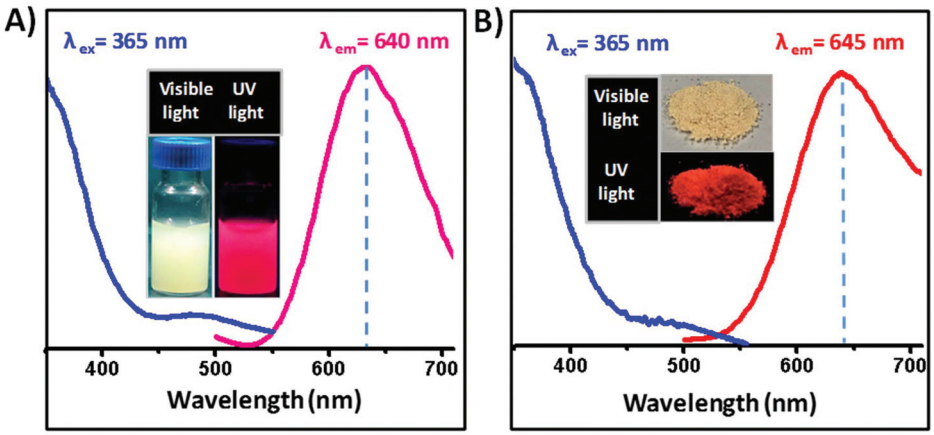

Fig. 3 Luminescence profile of DFNS@Au_{QC}BSA in the (A) solution and (B) solid states. Photographs of DFNS@Au_{QC}BSA in the solution and powder form under UV and visible light are shown in the respective insets. Both the samples were excited at 365 nm. The emission was found around 640 nm for the solution and around 645 nm for the solid state.

Resemblance of the luminescence spectrum with that of $Au_{QC}BSA$ in solution suggested that the clusters formed on the DFNS surface were essentially similar to that in the free state.[10]

The evolution of luminescence during the formation of the hybrid material was studied by measuring the time dependent PL spectra (Fig. S4†). After 4 h of synthesis, the mixture started to show faint luminescence and the color of the mixture also changed from slightly yellowish to light brown. This was an indication of the formation of the cluster. With time, a gradual increase in the luminescence intensity was observed along with a change in the color of the mixture. Maximum emission intensity was observed after 10 h of the reaction and the color of the reaction mixture turned golden brown. All the samples were excited at 365 nm and emission maxima were found to be around 640 nm. Luminescence of the hybrid material was stable and PL spectra up to 5 days are shown in Fig. S4.† The luminescence profile of the DFNS@Au_{QC}BSA at various stages of the reaction did not show any shift in its emission wavelength which suggested the formation of a stable species on DFNS.

Investigation of structural morphology of DFNS@Au_{QC}BSA using AFM

The formation of a hybrid material was further studied using atomic force microscopy (AFM). The 3D topographical images of DFNS and the hybrid material are presented in Fig. 4A and C, respectively. It clearly showed the significant changes in the morphology of the hybrid material as compared to their parent analogues. The height profile of a single DFNS particle was found to be 650 nm (Fig. 4B) while in the case of a single particle of the hybrid material, the height decreased to 320 nm (Fig. 4D).

We have mentioned in section 3.1 that during the growth of clusters on DFNS, the fibrous morphology of the latter was decreased due to etching of the surface. Although the exact reason is not apparent in this study, the reduced fibrous morphology could be the probable reason for the significant change in the height of the hybrid material.

Phase imaging provides complementary information on the topography and reveals the variations in the surface properties including the composition of the material. A large area phase image of the parent DFNS is shown in Fig. S5A† and the high resolution image of the edge of a DFNS is presented in Fig. S5B.† A thin sheet-like surface was observed in the parent DFNS which could be compared to the fibrous morphology as seen in the HRTEM image. But the hybrid material appeared to be completely different from the parent structure (Fig. S5C†). The thickness of the edge was increased, and it exhibited a brighter contrast which was absent in the case of parent DFNS (Fig. S5D†). The enhanced contrast was due to the presence of clusters at the edge of the hybrid material which was supported by the observation made by TEM EDS mapping.

XPS studies of DFNS@Au_{QC}BSA

X-ray photoelectron spectroscopy (XPS) helps to determine the oxidation state and binding properties of the protein stabilized gold clusters. XPS analysis of DFNS@Au_{QC}BSA confirmed the existence of the metallic state of gold. Au $4f_{7/2}$ appeared at 84.5 eV close to its Au^0 binding energy. The observed slightly higher binding energy (BE) could be contributed to its bonding environment. The S $2p_{3/2}$ and $2p_{1/2}$ BEs of 164.0 and 165.5 eV, respectively, are characteristic of thiolate.[12,34] This suggested that the cluster core is stabilized by the thiol groups

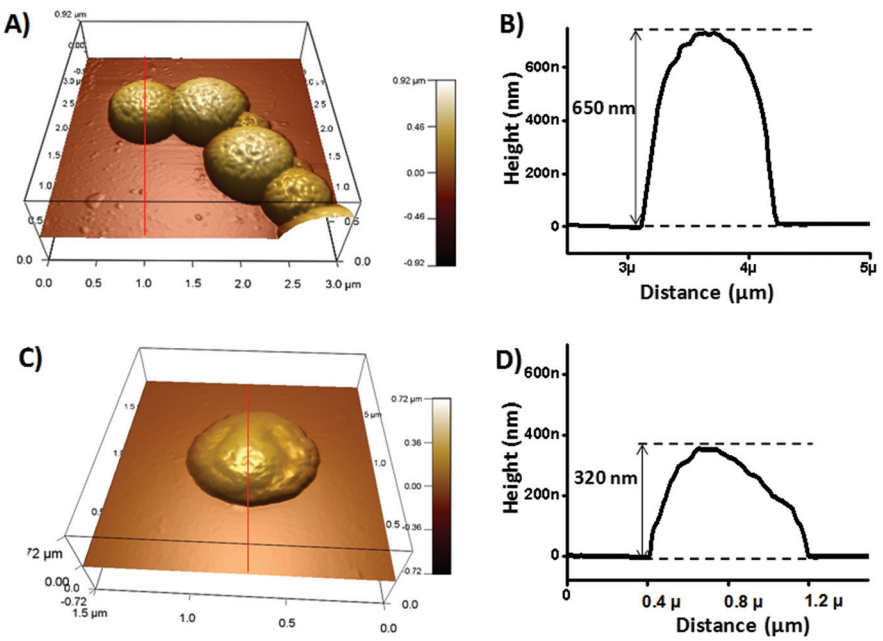

Fig. 4 The 3D topographical images of DFNS and the hybrid material are presented in (A) and (C), respectively. (B) and (D) Height profiles of DFNS and the hybrid material based on the line scans (labelled in red) in the AFM images, respectively.

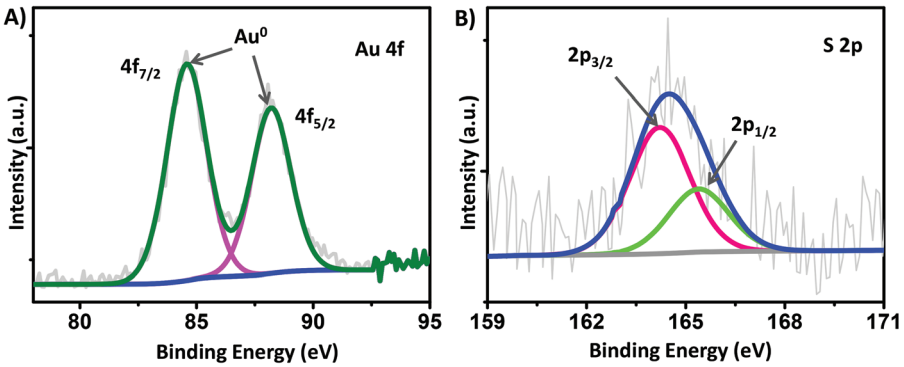

Fig. 5 XPS analysis of DFNS@Au_{QC}BSA showing metallic (A) Au 4f and thiolate (B) S 2p regions.

of the protein (mostly through the cysteine residues and are highly reactive, BSA has 35 cysteines). Slightly higher binding energy could be attributed to the oxidized state of sulphur, which is observed in the case of thiolate protected clusters upon X-ray exposure, thus leading to sulphite, sulphonate and sulphate species.[35,36] The cluster remained intact on DFNS as no Au^+ was observed. This is in agreement with the luminescence data also (Fig. 5).

Darkfield microscopy and metal ion sensing using DFNS@Au_{QC}BSA

The hybrid material, DFNS@Au_{QC}BSA, with distinct structural properties was observable under an optical microscope. For this analysis, a diluted solution of the sample was dropcast and dried on a glass slide. Dark field optical microscopy images of the parent DFNS appeared as spherical particles and a large area optical image of them is shown in Fig. 6A. The particles were subjected to hyperspectral imaging (HSI) analysis and the scattering spectrum of a single DFNS was collected (Fig. 6B). The corresponding single DFNS is provided in the inset of B in which the specific positions from where the spectra were collected are marked as 1 and 2. The scattering intensity was higher at the center than the edges and was due to the fibrous morphology, with decreasing density from the center towards the edge of the DFNS. Interestingly, the dark field image of the hybrid material was entirely different from

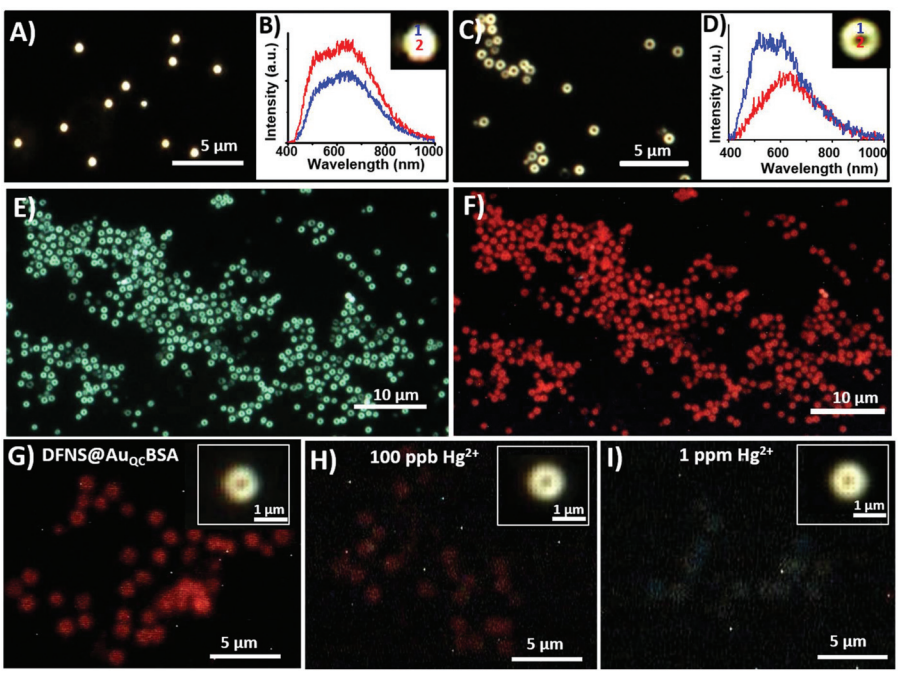

Fig. 6 Large area optical images of (A) DFNS and (C) DFNS@Au_{QC}BSA. The corresponding scattering spectra collected from the surface of DFNS and DFNS@Au_{QC}BSA are presented in (B) and (D), respectively. The positions in the single particle from where the spectra are collected are marked in the insets. (E) The white light and the corresponding (F) fluorescence image of DFNS@Au_{QC}BSA. (G–I) Fluorescence images of DFNS@Au_{QC}BSA, (G) before and after exposure to Hg^{2+} at concentrations of (H) 100 ppb and (I) 1 ppm, respectively. The corresponding optical images are shown in the insets.

that of the parent DFNS and appeared like hollow spheres or donuts (Fig. 6C).

Scattering spectra of the hybrid material were collected from similar positions as in the parent DFNS (Fig. 6D) and the corresponding single hybrid material particle is given in the inset. The results obtained were opposite to that of parent DFNS, where a higher scattering intensity was observed from the edge of the hybrid material compared to the center. The presence of clusters at the edges of the hybrid material results in such unique structure under an optical microscope which was strengthened by EDS mapping as well as AFM phase imaging. The increased electron density at the edges due to the clusters contributed to this enhanced scattering intensity. Fig. 6E shows a large area optical light image of the hybrid material and the corresponding fluorescence image is depicted in Fig. 6F. The fluorescence image exhibits red emission due to the clusters anchored on the surface of DFNS and similar hollow sphere structures were also observed in fluorescence images. Hg^{2+} is known to quench the luminescence of Au_{QC}@BSA and the interaction of Hg^{2+} with the core of the cluster has been suggested as the plausible reason for this quenching effect. In order to study the effect of Hg^{2+} on the luminescence of the hybrid material, different concentrations of Hg^{2+} were introduced to the former. Gradual disappearance of the luminescence intensity from the hybrid material upon addition of varying concentrations (100 ppb, 1 ppm) is shown in Fig. 6G–I. Though a significant decrease in the luminescence of the hybrid material was observable at 100 ppb of Hg^{2+}, a complete quenching of the luminescence occurred upon exposure to 1 ppm concentration of the Hg^{2+}. In both the cases, the optical images of the hybrid material remained unaffected as shown in the inset of Fig. 6H and I as scattering intensity was nearly the same. It suggested that even at higher concentration of Hg^{2+}, the structure of the material was not affected. Parent DFNS was not luminescent and a large area optical image and the corresponding fluorescence image of DFNS are shown in Fig. S6A and S6B,† respectively. Different concentrations of Hg^{2+} were introduced to the parent DFNS and optical images were captured. No structural changes were observed. Thus, it can be confirmed that the quenching effect was due to the clusters alone. This approach is advantageous over the solution phase method as single particle level investigations are possible.

Conversion of silane to silanol by DFNS@Au_{QC}BSA

DFNS acts as an excellent material to support metal nanoparticles and organometallic complexes to design nanocatalysts.[27] This prompted us to use the hybrid material (DFNS@Au_{QC}BSA) for the oxidation of organosilanes to silanols. The silane to silanol reaction was performed in a tetrahydrofuran THF–water mixture at 45 °C using 5 mg of the hybrid material as the catalyst as shown in scheme Fig. 7A. The result showed that these clusters were catalytically active (Fig. 7B). The catalyst showed higher kinetics for dimethylphenylsilane as compared to other silanes with 77% of silane to silanol conversion in 10 h. For other silanes, kinetics as well as conversion dropped as a function of neighbouring functional group of the silane molecule. For both triisopropylsilane and tributylsilane, 42% silane was converted to silanol while for triphenylsilane, only 19% conversion was observed and such reduced conversion rate could be attributed to the steric hindrance caused due to the presence of the bulky phenyl group. To study the catalytic effect of the hybrid material, the conversion of dimethylphenylsilane to dimethylphenylsilanol reaction was performed at 45 °C in the presence and absence of light (>385 to 740 nm) but no significant improvement was observed as compared to the conventional reaction without light (Fig. S7†). To maximize the effect of light on the catalysis reaction, temperature was reduced to 30 °C and in this case, it was possible to differentiate the effect of light on the catalysis

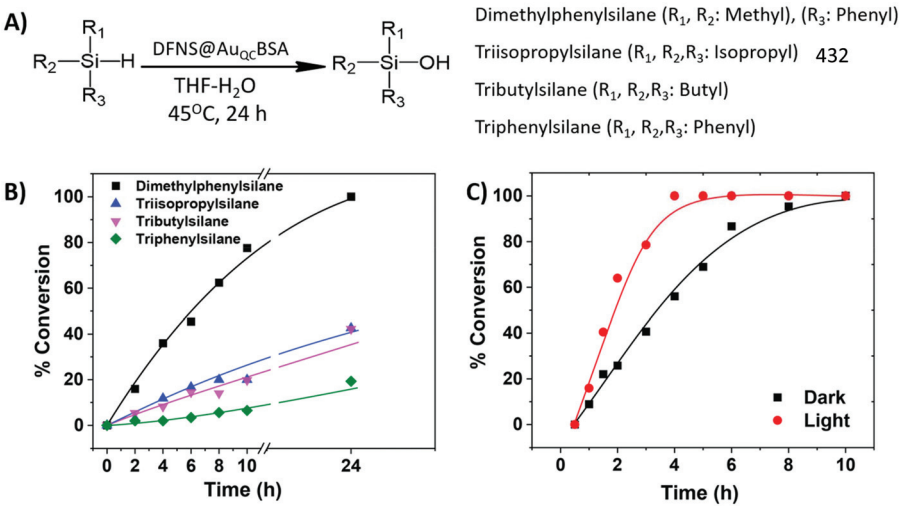

Fig. 7 (A) The reaction scheme showing the conversion of silane to silanol. (B) The conversion of various silanes to silanol at 45 °C during different time intervals. (C) The effect of light for the dimethylphenylsilane to dimethylphenylsilanol conversion reaction, at 30 °C (error in the catalytic measurements is ±5%).

as compared to the reaction conducted in the dark at 30 °C (Fig. 7C). In the presence of light, the reaction occurred much faster (100% conversion in 4 h) while only 56% conversion was observed without light at 4 h. There was no role of the enzyme in the silane hydrolysis reaction which was confirmed by controlled catalytic experiments using DFNS and BSA complex, in which no catalytic activity was found under similar experimental conditions. Thus, the enhancement could be directly attributed to the presence of clusters.

UV-Vis absorption spectra of DFNS@Au_{QC}BSA were measured in the presence and absence of light, after the catalytic reaction (Fig. S8†). In both the cases, a plasmonic peak around 532 nm was found which was absent before the catalytic activity (Fig. S1B†). This clearly suggested the change in the size of the cluster after catalysis. It showed that the catalytic conditions made gold clusters to aggregate.

Conclusions

In conclusion, we have developed a luminescent hybrid material (DFNS@Au_{QC}BSA) using Au_{QC}@BSA loaded on DFNS which can act both as a chemical sensor and a catalyst. Utilizing the scattering and luminescence properties, imaging of such mesostructures was performed and they were used for sensing Hg^{2+}. This approach enabled a single particle luminescence imaging with a unique donut like mesostructure. The hybrid material was demonstrated as the catalyst in the oxidation of organosilanes to silanols, with higher kinetics of 77% conversion for dimethylphenylsilane to dimethylphenylsilanol. The efficiency of the catalyst was found to increase in the presence of light when the reaction was performed at 30 °C and 100% conversion was achieved only in 4 h. The hybrid material has great potential in numerous applications in various fields using combined properties of the luminescent clusters and DFNS. Additional experiments are required to understand the system in more detail and to improve the sensitivity of detection as well as the catalytic efficiency of the material.

Conflicts of interest

There are no conflicts to declare.

Acknowledgements

We thank the Department of Science and Technology, Govt. of India for their continuous support on our research program on nanomaterials. V. P. thanks the Department of Atomic Energy, Govt. of India for funding. J. S. M. thanks Council of Scientific and Industrial Research (CSIR) for her research fellowship. T. A. and P.S. thank IIT Madras for their research fellowship.

Notes and references

1 R. Jin, *Nanoscale*, 2010, **2**, 343–362.
2 A. Mathew and T. Pradeep, *Part. Part. Syst. Charact.*, 2014, **31**, 1017–1053.
3 P. L. Xavier, K. Chaudhari, A. Baksi and T. Pradeep, *Nano Rev.*, 2012, **3**, 14767–14782.
4 D. M. Chevrier, A. Chatt and P. Zhang, *J. Nanophotonics*, 2012, **6**, 064504-1–064504-16.
5 Q. Yao, Z. Wu, Z. Liu, Y. Lin, X. Yuan and J. Xie, *Chem. Sci.*, 2021, **12**, 99–127.
6 I. Chakraborty and T. Pradeep, *Chem. Rev.*, 2017, **117**, 8208–8271.
7 J. T. Petty, J. Zheng, N. V. Hud and R. M. Dickson, *J. Am. Chem. Soc.*, 2004, **126**, 5207–5212.
8 C. He, P. M. Goodwin, A. I. Yunus, R. M. Dickson and J. T. Petty, *J. Phys. Chem. C*, 2019, **123**, 17588–17597.
9 J. Zheng, J. T. Petty and R. M. Dickson, *J. Am. Chem. Soc.*, 2003, **125**, 7780–7781.
10 J. Xie, Y. Zheng and J. Y. Ying, *J. Am. Chem. Soc.*, 2009, **131**, 888–889.
11 A. Mathew, P. R. Sajanlal and T. Pradeep, *J. Mater. Chem.*, 2011, **21**, 11205–11212.
12 P. L. Xavier, K. Chaudhari, P. K. Verma, S. K. Pal and T. Pradeep, *Nanoscale*, 2010, **2**, 2769–2776.
13 A. Baksi, P. L. Xavier, K. Chaudhari, N. Goswami, S. K. Pal and T. Pradeep, *Nanoscale*, 2013, **5**, 2009–2016.
14 A. Baksi and T. Pradeep, *Nanoscale*, 2013, **5**, 12245–12254.
15 H. Li, W. Zhu, A. Wan and L. Liu, *Analyst*, 2017, **142**, 567–581.
16 J. Xie, Y. Zheng and J. Y. Ying, *Chem. Commun.*, 2010, **46**, 961–963.
17 N. Goswami, A. Giri, M. S. Bootharaju, P. L. Xavier, T. Pradeep and S. K. Pal, *Anal. Chem.*, 2011, **83**, 9676–9680.
18 M. A. Habeeb Muhammed, P. K. Verma, S. K. Pal, A. Retnakumari, M. Koyakutty, S. Nair and T. Pradeep, *Chem. – Eur. J.*, 2010, **16**, 10103–10112.
19 L. Trasande, P. J. Landrigan and C. Schechter, *Environ. Health Perspect.*, 2005, **113**, 590–596.
20 A. Ghosh, V. Jeseentharani, M. A. Ganayee, R. G. Hemalatha, K. Chaudhari, C. Vijayan and T. Pradeep, *Anal. Chem.*, 2014, **86**, 10996–11001.
21 Y.-Q. Wang, T. Zhao, X.-W. He, W.-Y. Li and Y.-K. Zhang, *Biosens. Bioelectron.*, 2014, **51**, 40–46.
22 N. Mohammed, A. Baidya, V. Murugesan, A. A. Kumar, M. A. Ganayee, J. S. Mohanty, K. C. Tam and T. Pradeep, *ACS Sustainable Chem. Eng.*, 2016, **4**, 6167–6176.
23 A. Upadhyay and C. P. Rao, *ACS Appl. Mater. Interfaces*, 2019, **11**, 7965–7973.
24 Y. Okada, M. Oba, A. Arai, K. Tanaka, K. Nishiyama and W. Ando, *Inorg. Chem.*, 2010, **49**, 383–385.
25 W. Li, A. Wang, X. Yang, Y. Huang and T. Zhang, *Chem. Commun.*, 2012, **48**, 9183–9185.
26 K. B. Sharpless, *Angew. Chem., Int. Ed.*, 2002, **41**, 2024–2032.

27 A. Maity and V. Polshettiwar, *ChemSusChem*, 2017, **10**, 3866–3913.
28 A. Maity, A. Das, D. Sen, S. Mazumder and V. Polshettiwar, *Langmuir*, 2017, **33**, 13774–13782.
29 R. Singh, R. Belgamwar, M. Dhiman and V. Polshettiwar, *J. Mater. Chem. B*, 2018, **6**, 1600–1604.
30 J. S. Mohanty, K. Chaudhari, S. Chennu and T. Pradeep, *J. Phys. Chem. C*, 2019, **123**, 28969–28976.
31 H. W. Li, Y. Yue, T. Y. Liu, D. Li and Y. Wu, *J. Phys. Chem. C*, 2013, **117**, 16159–16165.
32 A. Baksi, A. Mitra, J. S. Mohanty, H. Lee, G. De and T. Pradeep, *J. Phys. Chem. C*, 2015, **119**, 2148–2157.
33 M. W. Sabaa, D. H. Hanna, M. H. Abu Elella and R. R. Mohamed, *Mater. Sci. Eng., C*, 2019, **94**, 1044–1055.
34 G. J. Ashwell, B. U. Wojcik and L. J. Phillips, *Angew. Chem., Int. Ed.*, 2010, **49**, 3508–3512.
35 T. Laihoa, J. A. Leiroa and J. Lukkarib, *Appl. Surf. Sci.*, 2003, **212–213**, 525–529.
36 X. L. Guével, B. Hötzer, G. Jung, K. Hollemeyer, V. Trouillet and M. Schneider, *J. Phys. Chem. C*, 2011, **115**, 10955–10963.